ELSEVIER

Contents lists available at ScienceDirect

Journal of Controlled Release

journal homepage: www.elsevier.com/locate/jconrel





Succinate based polymers drive immunometabolism in dendritic cells to generate cancer immunotherapy

Sahil Inamdar ^{a,e}, Abhirami P. Suresh ^b, Joslyn L. Mangal ^b, Nathan D. Ng ^c, Alison Sundem ^a, Hoda Shokrollahzadeh Behbahani ^a, Thomas E. Rubino Jr ^{h,i}, Xiaojian Shi ^d, Sharon T. Loa ^f, Jordan R. Yaron ^b, Taro Hitosugi ^f, Matthew Green ^{a,j}, Haiwei Gu ^{d,g}, Marion Curtis ^{f,h,i}, Abhinav P. Acharya ^{a,b,j,k,l,m,*}

- ^a Chemical Engineering, School for the Engineering of Matter, Transport, and Energy, Arizona State University, Tempe, AZ 85281, USA
- b Biological Design, School for the Engineering of Matter, Transport, and Energy, Arizona State University, Tempe, AZ 85281, USA
- ^c Molecular Biosciences and Biotechnology, The College of Liberal Arts and Sciences, Arizona State University, Tempe, AZ 85281, USA
- ^d College of Health Solutions, Arizona State University, Phoenix, AZ 85004, USA
- ^e Department of Immunology, Mayo Clinic, Scottsdale, AZ 85259, USA
- f Department of Oncology, Mayo Clinic, Rochester, MN 55905, USA
- g Center for Translational Science, Florida International University, Port St. Lucie, FL 34987, USA
- h Department of Cancer Biology, Mayo Clinic, Scottsdale, AZ 85259, USA
- i College of Medicine and Science, Mayo Clinic, Scottsdale, AZ 85259, USA
- ^j Biomedical Engineering, School of Biological and Health Systems Engineering, Arizona State University, Tempe, AZ 85281, USA
- k Materials Science and Engineering, School for the Engineering of Matter, Transport, and energy, Arizona State University, Tempe, AZ 85281, USA
- 1 Biodesign Center for Immunotherapy, Vaccines and Virotherapy, Arizona State University, Tempe, AZ 85281, USA
- ^m Biodesign Center for Biomaterials Innovation and Translation

ARTICLE INFO

Keywords: Cancer Succinate Metabolism Immune system Vaccine Dendritic cells

ABSTRACT

Boosting the metabolism of immune cells while restricting cancer cell metabolism is challenging. Herein, we report that using biomaterials for the controlled delivery of succinate metabolite to phagocytic immune cells activates them and modulates their metabolism in the presence of metabolic inhibitors. In young immuno-competent mice, polymeric microparticles, with succinate incorporated in the backbone, induced strong proinflammatory anti-melanoma responses. Administration of poly(ethylene succinate) (PES MP)-based vaccines and glutaminase inhibitor to young immunocompetent mice with aggressive and large, established B16F10 melanoma tumors increased their survival three-fold, a result of increased cytotoxic T cells expressing RORγT (Tc17). Mechanistically, PES MPs directly modulate glutamine and glutamate metabolism, upregulate succinate receptor SUCNR1, activate antigen presenting cells through and HIF-1alpha, TNFa and TSLP-signaling pathways, and are dependent on alpha-ketoglutarate dehydrogenase for their activity, which demonstrates correlation of succinate delivery and these pathways. Overall, our findings suggest that immunometabolism-modifying PES MP strategies provide an approach for developing robust cancer immunotherapies.

1. Introduction

Therapeutics that modulate immune cell metabolism have achieved major success in cancer research. [1–4] Notably, activating innate immune cells such as dendritic cells (DCs) and macrophages (M\$\phi\$s) requires the modulation of metabolic intermediates and metabolic pathways. [5–9] The accumulation of metabolic intermediates has the potential to regulate immune responses and could play a role in disease progression,

such as inflammation caused by tumors. ⁹ For example, cancer vaccines activate DCs and tumor-associated M\$\phi\$s (TAMs) by modulating their energy metabolism (e.g., glycolysis, glutaminolysis, Krebs cycle). [10] Immune cells' metabolic demands change along with changes in their activation status. [11,12] It has been observed that immune-cell metabolism adapts to match these demands, metabolically shifting through the increased expression of nutrient transporters and oxidative phosphorylation pathways. [13] For example, when activated DCs and M\$\phi\$s

^{*} Corresponding author at: 550 GWC, 651 E. Tyler Mall, Tempe, AZ, USA. *E-mail address*: abhi.acharya@asu.edu (A.P. Acharya).

upregulate glucose and glutamine transporters, this enables downstream signaling and the production of pro-inflammatory proteins. [14,15]

Like activated immune cells, cancer cells also upregulate glucose and glutamine transporters for proliferation and survival. In fact, hyperactivation of cancer-cell metabolism is a direct result of the modulation of intracellular signaling pathways that are disrupted by mutated oncogenes and tumor-suppressor genes. [16] Cancer cells preferentially uptake and convert glucose into lactate even in the presence of sufficient oxygen, known as the Warburg effect. [17,18] Recent studies observed that glutamine is an essential bioenergetic and anabolic substrate for many cancer cell types. [16] Cancer cells exhibiting aerobic glycolysis rely on glutamine as well as glucose as the carbon source. [19,20] Glutamine is used to provide intermediates of the Krebs cycle to feed biosynthetic pathways as precursors. [21] Therefore, cancer cells are dependent on glutamine for survival and proliferation. [22,23] Cancer cells have accelerated energy metabolism, which has been exploited as a target for various therapeutic studies. [24,25] In clinical trials, blocking the glutaminase pathway has been used to treat melanoma, squamous cell carcinoma, and other solid tumors. [26–29]

Glutaminolysis feeds into the Krebs cycle and generates metabolites such as succinate. [5] Succinate is associated with an inflammatory response in innate immune cells. [30,31] Also, succinate is synthesized within the mitochondria and converted to fumarate in the TCA cycle. [32] The succinate receptor SUCNR1 is present on the cell surface and expressed in myeloid cells such as DCs and M\ps. [32,33] Recent studies

suggest that, when succinate accumulation activates SUCNR1, it increases inflammatory cytokine production in both human and mouse DCs. [33] Moreover, succinate accumulation results in increased IL-1 β secretion, an effect that was lost in SUCNR1-deficient mice. [34,35] Succinate's inflammatory effect can thus be used to effectively modulate immune-cell metabolism and generate pro-inflammatory immunotherapy. [36] Phagocytes (DCs and M\$\phi\$s) can sample foreign material like synthetic particles. [37,38] Therefore, particles that are able to deliver metabolites such as succinate to these phagocytic cells may be able to modulate immune-cell metabolism. [38,39]

This study describes an immunometabolism strategy based on the sustained release of succinate from biomaterials, which incorporate succinate in the polymer's backbone (Fig. 1a). These succinate-based polymers allow phagocytes to perform their metabolic function in the presence of chemotherapeutics. Sustained release of succinate not only modulates the metabolism of innate immune cells but also induces a proinflammatory phenotype in these cells, resulting in effective cancer immunotherapy. This vaccine formulation was tested in young melanoma mouse model.

2. Results and discussion

Condensation polymerization was used to generate biomaterials capable of sustained succinate delivery and thus provide a continuous effect on metabolism. Polyesters were generated by reacting succinate

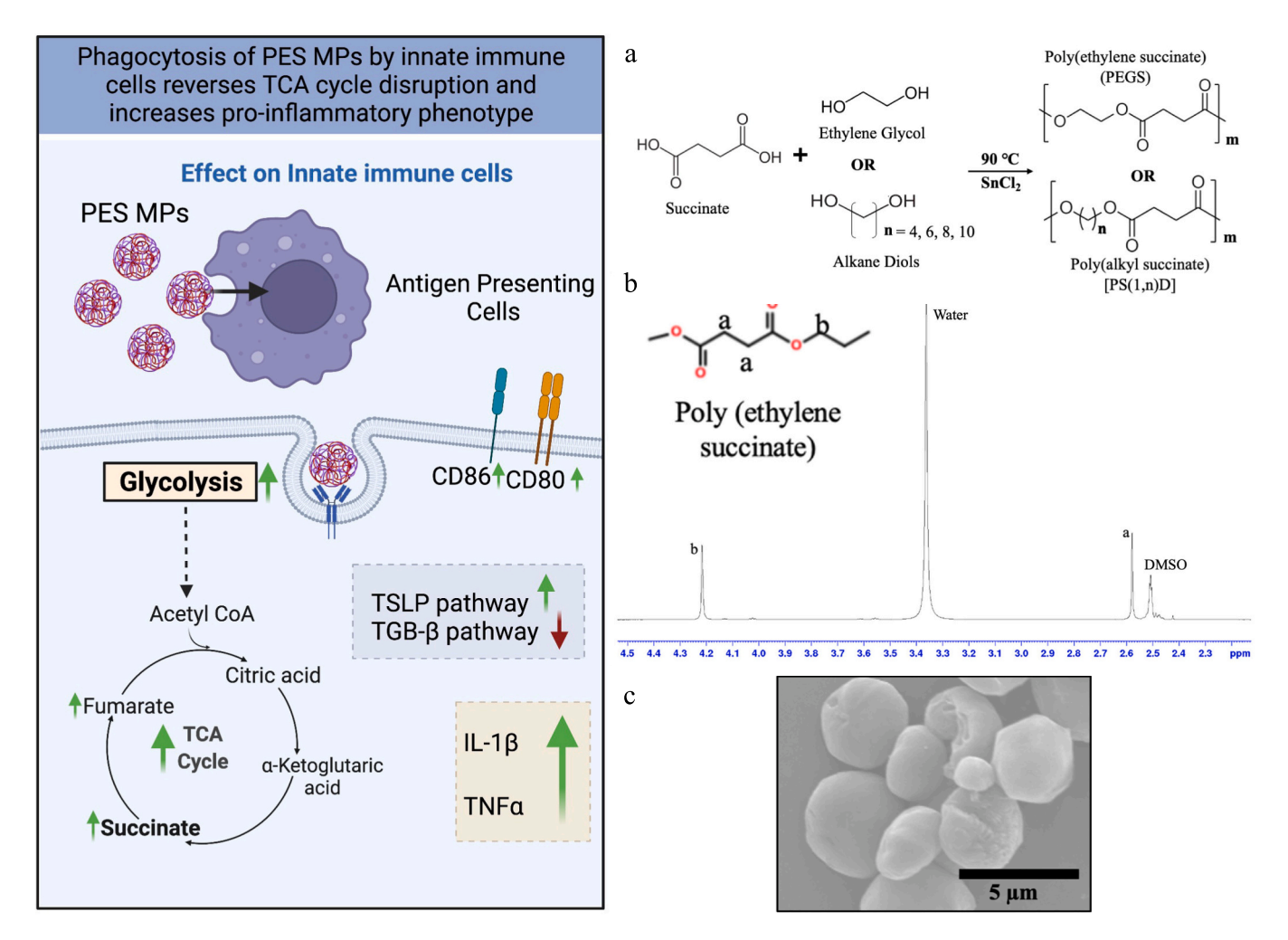


Fig. 1. Succinate, an alarmin, can be formulated into polymeric microparticles (MPs). Schematic representation of antigen presenting cell phagocytosing MPs generated using PES polymer is shown. a. Reaction schematic of formulation of succinate-based polymers b. ¹H NMR of PES polymer. c. Scanning electron microscopy (SEM) images indicate a spherical morphology for the PES MPs of different sizes.

with aliphatic diols (Fig. 1b,c Supplementary Figs. S1) with their molecular weights ranging from 6 kDa - 10 kDa. These polymers were then formulated into MPs to control intracellular or extracellular delivery of succinate. Scanning electron microscopy (SEM) indicated a spherical morphology for MPs of different sizes (Fig. 1d,e Supplementary Fig. S2).

For the smaller particles, average MP diameters between 1 and 3 μm were observed using dynamic light scattering (DLS) (Supplementary Fig. S3, S4). Notably, PES MPs released ~2-fold higher succinate compared to other succinate polymers in 30 days, potentially due to PES MPs' lower hydrophobicity (Supplementary Fig. S5). Therefore, PES MPs were used for all subsequent experiments. Next, the DCs' phagocytosis was investigated using confocal microscopy. It was determined that bone marrow-derived DCs (BMDCs) successfully phagocytosed the PES MPs (Fig. 2a; Supplementary Fig. S6). Minimal phagocytosis was observed when DCs were incubated at 4 °C. Also, no significant pH changes in the cell culture media were observed after a 24-h incubation of these particles, which suggests that the cells should be able to buffer the endosome containing PES MPs (Supplementary Fig. S7). Moreover, it was observed that PES MPs' uptake by DCs in vitro was 92.75 \pm 3% in 24 h. Next, a ¹³C tracing flux assay was used to investigate the metabolic pathways where succinate released from PES MPs is metabolized. Specifically, ¹³C-PES MPs generated from a ¹³C succinate-based PES polymer were used to analyze 28 different TCA cycle-associated metabolites and thus trace the intracellular path of the MPs (Fig. 2b). Upon treatment with $^{13}\text{C-PES}$ MPs, the PES MPs intracellularly release succinate and enter the TCA cycle, as indicated by a significant increase in the ¹³C succinate levels as compared to untreated or soluble (sol.) ¹³C succinate treated groups. The PES MPs were further metabolized into other metabolites associated with the TCA cycle, such as fumarate and malate. This suggests that succinate delivered to DCs intracellularly enters the TCA cycle (Fig. 2c, Supplementary Fig. S8). This can be attributed to DCs' ability to better internalize particles as compared to soluble ligands. [40] Additionally, tracing experiments suggest that the ¹³C succinate is metabolized to pyruvate, aspartate, and homoserine, indicating further downstream changes. Furthermore, there was increased incorporation of ¹³C succinate carbon into glutamine, which suggests that the PES MPs can potentially directly metabolize and modulate the glutaminase pathway.

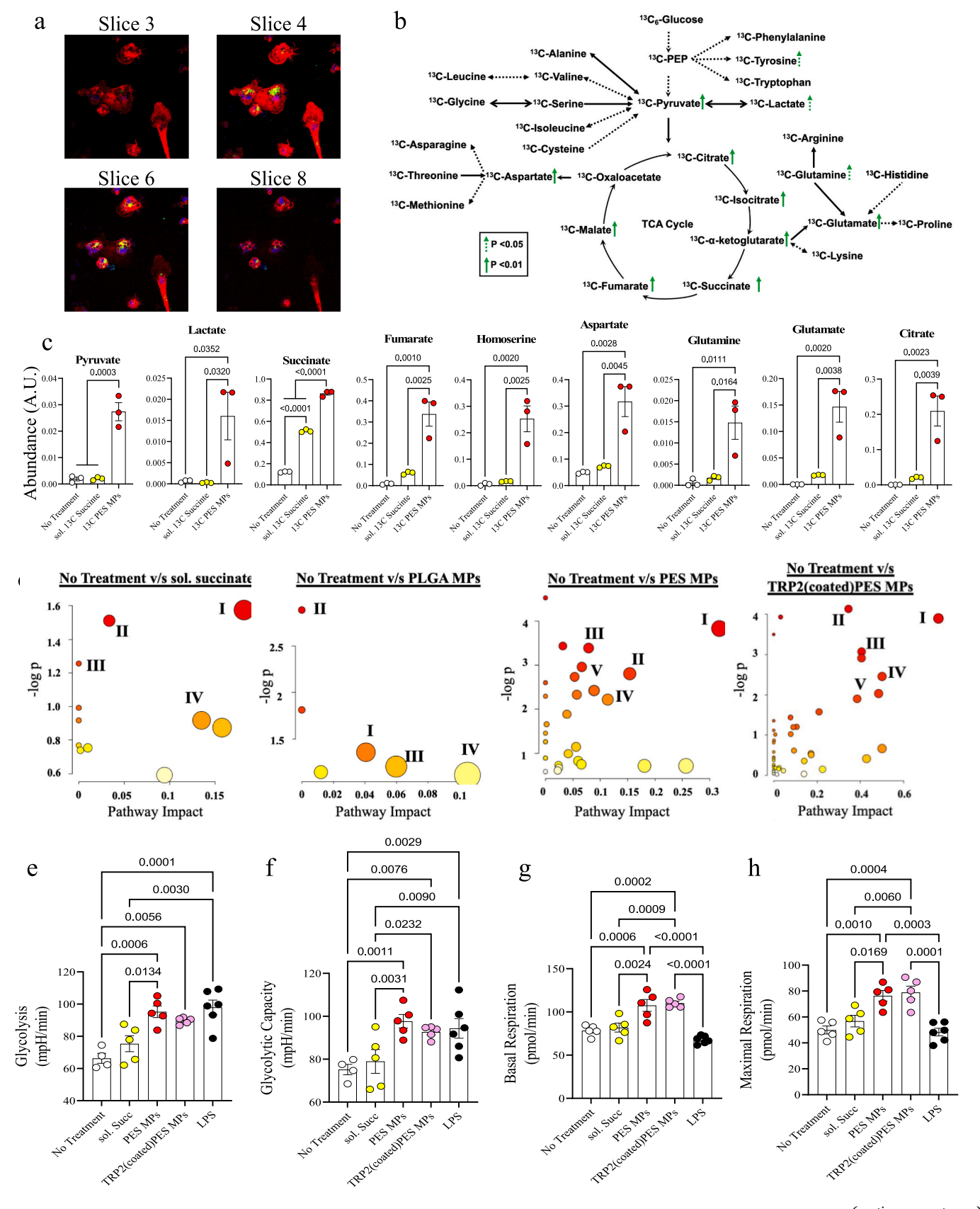
Next, to further investigate how PES MPs modulate DC metabolism, changes in the intracellular metabolite profile were studied using abundance data metabolomics. [41] Interestingly, a significant increase in metabolites was observed in the serine metabolism pathway. Fatty acid elongation and glyoxylate metabolism, thus suggesting that PES MPs might be able to support pro-inflammatory DC metabolic phenotype, which further confirms the flux tracing analysis (Fig. 2d, Supplementary Fig. S9). [5,42-44] Similar pathways were modulated in DCs treated with LPS, a known pro-inflammatory stimulator suggesting the pro-inflammatory behaviour of PES MPs (Supplementary Fig. S9). [45,46] To further study the metabolism of succinate-based MPs, an inhibitor that restricts conversion of aKG to succinate was utilized (Supplementary Fig. S9). [47–49] It was observed that, similar pathways were modulated in DCs treated with iaKGDH and iaKGDH + PES MPs when compared to untreated DCs, respectively. Also, these pathways were distinct as compared to pathways modulated in DCs treated with PES MPs indicating that effect of PES MPs is mitigated if iaKGDH is added in the presence of PES MPs. Moreover, PES MPs were coated with a melanoma antigen, tyrosine related protein 2 (TRP2), to study the modulations in DC metabolism (Fig. 2d, Supplementary Fig. S10). A significant increase in the D-glutamine and glutamate metabolism was observed, along with arginine and glutathione metabolism, indicating the upregulation of pro-inflammatory phenotypic pathways.

Activated DCs are known to upregulate energy-associated pathways such as glycolysis and oxidative phosphorylation. [6] Therefore, to test whether PES MPs modulate energy-associated pathways, Seahorse extracellular flux assays were used (Fig. 2e-h, Supplementary Fig. S11). Soluble succinate with equivalent amount that was released from

particles at 24 h was utilized as control. A significant increase in the glycolysis and glycolytic capacity of DCs treated with PES MPs was observed as compared to other treatment groups (Fig. 2e,f). A significant upregulation of basal and maximal respiration in DCs treated with PES MPs, as compared to other treatment groups, was also observed (Fig. 2g, h). These results indicate the upregulation of these energy-associated pathways, suggesting that treatment with PES MPs can lead to DC activation. Furthermore, the effect of a glutaminase 1 inhibitor (GLS1), CB-839, which is known to disrupt the TCA cycle, [29,50] on the energy associated pathways was also studied using Seahorse extracellular flux assays (Supplementary Fig. S12). The maximal respiration in CB-839treated DCs significantly decreased as compared to the no-treatment control. There was a significant increase in the basal and maximal respiration in CB-839 and PES MP-treated DCs, as compared to untreated or CB-839 treated DCs. In all cases, DCs were first treated with CB-839 and then treated with PES MPs, ensuring that the glutaminase pathway was downregulated prior to any treatment. Overall, these data indicate that PES MPs upregulate DC mitochondrial respiration in the presence of CB-839. Similar results were observed in TRP2(coated)PES MP-treated DCs, in vitro, suggesting that these TRP2(coated)PES MPs can also support DC function (Fig. 2e-h; Supplementary Fig. 12).

This pro-inflammatory metabolic phenotype in DCs treated with PES MPs was also accompanied by significant upregulation in inflammationassociated RNA molecules as determined by qRT-PCR (Fig. 3a-c; Supplementary Fig. S13). DCs treated with PES MPs also showed a \sim 7-fold increase in SUCNR1 (succinate receptor), a \sim 14-fold increase in TNF- α , and a \sim 550-fold increase in IL-1 β mRNA-level as compared to untreated DCs. Significant increases in mRNA-levels of SUCNR1 (3-fold), TNF-α (8fold) and IL-1β (500-fold) were observed in DCs treated with PES MPs as compared to DCs treated with the monomers alone. Furthermore, the mRNA levels of SUCNR1 significantly increased (5-fold) in DCs treated with both PES MPs and CB-839 as compared to those treated with CB-839 alone. Although an increase in SUCNR1 expression was seen, this does not directly indicate that succinate delivery leads to SUCNR1 expression, and this increase might be due to the activation of antigenpresenting cells. [51] There was a significant 4-fold increase in the hypoxia-inducing factor- 1α (HIF- 1α), in CB-839 + PES MP treated DCs as compared to DCs treated with CB-839 only. Recent studies show that HIF-1α activation in macrophages induces activation through upregulation of the hypoxia pathway. [52-54] Moreover, there was also a significant upregulation of NLRP3 (~2-fold) and IL-1\beta (~25-fold), markers of DC activation, in the DCs treated with CB-839 + PES MPs as compared to the CB-839 control. Concurrently, treatment of CB-839 + PES MP also triggered a significant upregulation of the proinflammatory TNF α (~6-fold) when compared to the CB-839 control. Importantly, modulation of TNFα has been shown to be independent of NLRP3 expression, suggesting that PES MPs act as alarmins and can stimulate multiple damage-associated molecular patterns (DAMPs) in DCs. [55,56] Notably, PES MPs upregulate signaling pathways and RNA molecules in DCs when compared to the controls of PLGA MPs or no treatment control. These pathways were different in LPS treated DCs as compared to no treatment control. These data indicate that PES MPs activated DCs through a different pathway as compared to LPS.

To further investigate PES MPs' effect on modulating DC activation pathways, bulk RNA sequencing was performed (Fig. 3d,e and S14, S15). There was a significant upregulation in the EGF/EGFR- and EGFR1-signaling pathways in DCs treated with PES MPs as compared to untreated DCs or those treated with soluble succinate. This upregulation can be attributed to the increase in G-protein-coupled receptors (GPCRs) as they play an important role in the EGF receptor's transactivation. [57] Activated EGFR is known to recruit various cytoplasmic proteins that transduce and regulate the EGFR function; this eventually leads to the upregulation of extracellular signal-regulated kinase (ERK) and its downstream pathways, indicating increase in cell migration, activation, and proliferation phenotype of these DCs. [58] Furthermore, there was a significant increase in the thymic stromal lymphopoietin (TSLP)



(caption on next page)

Fig. 2. PES MPs modulate DC metabolism, *in vitro*. a. Confocal microscopy image slices in the z-directon indicates internalization of FITC-PES MPs by DCs (Scale bar = 70 μm. blue = nucleus; red = cytoplasm; green = FITC-PES MPs; yellow = red+green; Supplementary Fig.S6 for more information). b. Schematic representation of path traced by ¹³C Succinate upon its intracellular release by ¹³C-PES MPs. c. Significant increase in 13C succinate was observed in the intracellular metabolic concentration as compared to untreated or 13C succinate treated DCs; y-axis indicates fractional enrichment (*n* = 3; One-way ANOVA, Tukey-test) d. Metabolomics study indicates specific pathways being modulated in DCs significantly (No Treatment v/s sol. Succinate: I – Amino sugar and nucleotide sugar metabolism, II – Valine, Leucine, and isoleucine degradation, III – Valine, Leucine, and isoleucine biosynthesis and IV. Starch and sucrose metabolism; No Treatment v/s PLGA MPs: I – Propanoate metabolism, II – Glycine, serine, and threonine metabolism, III – Cysteine and methionine metabolism and IV – Tryptophan metabolism; No Treatment v/s PES MPs: I – Serine Metabolism, II – Fatty acid elongation, III – Glyoxylate metabolism, IV – Tryptophan metabolism and V – TCA cycle; PLGA MPs v/s PES MPs: I – Nicotine and nicotinamide metabolism, II – Pentose phosphate pathway, III – Tryptophan metabolism and IV – Butanoate metabolism; No Treatment v/s TRP2 (coated)PES MPs: I – Alanine, aspartate, and glutamate metabolism, II – Arginine biosynthesis, III – Glutathione metabolism and IV – D-Glutamine and D-glutamate metabolism (*n* = 3; Unpaired *t*-test with Welch's correction). The size of the circle signify the level of modulation and the colour from yellow to red signify the level of significance between the compared groups. e., f., g., h., Significant upregulation of glycolysis (e), glycolytic capacity (f), basal respiration (g), and maximal respiration (h) was observed in DCs treated with PES and TRP2(coated)PES MPs as compared to other

pathway, along with the IL-7-signaling pathway in DCs treated with PES MPs. TSLP signals through a complex containing IL-7 receptor α and can activate multiple signaling transduction pathways, including the JAK/ STAT and PI-3 kinase pathway. When activated, these pathways are mainly responsible for cellular metabolism, proliferation, growth, and survival, [59,60] further indicating PES MPs' ability to modulate and activate DCs. Specifically, there was significant upregulation of Slc16a12, Peg10 and srgn in DCs treated with PES MPs as compared to untreated or soluble succinate-treated DCs. Studies suggest that the Slc16a12 gene plays a substantial role in the transport of monocarboxylic acids. [61,62] An upregulation of Slc16a12 can indicate the transportation of cleaved succinate from the polymeric MPs. Additionally, a recent study reported that DCs transfected with Peg10 adenovirus elicit an anti-tumor immune response in vitro as well as in vivo. Overall, these data suggest that PES MPs can modulate DC function by transactivation of various activation pathways.

Next, PES MPs' ability to modulate DC protein expressions was observed using flow cytometry (Fig. 3f-h; Supplementary Fig. S16). Primarily, it was observed that DCs' cell viability upon treatment with PES MPs was >95% (Supplementary Fig. S16). Furthermore, DCs treated with PES MPs were able to significantly upregulate their activation as indicated by the ~4-fold increase in the frequency of MHCII+CD86+ of CD11c⁺ cells as compared to other treatment groups (Fig. 3f). To determine whether DC activation was due to PES MPs' intracellular delivery of succinate, DCs were treated with soluble succinate and soluble ethylene glycol (monomers used for PES synthesis). No DC activation was observed upon treatment with monomers for 24 h, indicating that the MPs are required for DC activation. Similarly, to confirm that DC activation was not due to the phagocytosis process alone, DCs were treated with PLGA MPs and PLGA MPs + sol. Succinate as controls. However, no DC activation was observed upon these treatments, suggesting that phagocytosis and the intracellular release of succinate by PES MPs are required to activate DCs. Additionally, DCs treated with TRP2(coated)PES MPs showed significant upregulation in DC activation, as indicated by a \sim 3-fold increase in the MHCII⁺CD86⁺ of CD11c⁺ cells as compared to the controls (Fig. 3g). Activation significantly increased (~3-fold) in DCs treated with CB-839 + TRP2(coated)PES MPs as compared to other treatment groups, suggesting that these MPs can activate DCs in the presence of an inhibitor (Fig. 3h).

DCs activated by PES MPs were also able to produce proinflammatory cytokines (essential for generating anti-tumor responses [63–65]), with an 11-fold increase in TNF α protein production as compared to the no-treatment control (Supplementary Fig. S17). Moreover, a 13-fold increase in TNF α concentration in the DCs treated with CB-839 + PES MPs was observed as compared to the CB-839-only treatment, indicating a strong pro-inflammatory response. Concurrently, upon intracellular cytokine staining of IL-10 (anti-inflammatory cytokine), IL-12p70, and TNF α (pro-inflammatory cytokines), a significant upregulation of IL-12p70+ (~6-fold) and TNF α + (~4-fold) and a significant decrease in IL-10+ (~9-fold) frequency was observed in the

DCs treated with PES MPs as compared to the untreated controls (Supplementary Fig. S17). Also, the PES MPs had undetectable levels of endotoxin (<0.01 EU/mL), suggesting that the activation of DCs was not due to endotoxins. Overall, these data indicate that PES MPs led to activation of DCs and that DC activation (as observed by CD86 expression) was dose-dependent, increasing along with increased concentration of PES MPs (Supplementary Fig. S18). Also, it was observed that PES MPs were able to activate DCs, even when these DCs were pre-treated with increasing concentrations of CB-839, indicating their activation potency in the presence of GLS1 inhibition (Supplementary Fig. S18). To further study PES MPs' immunomodulatory effect on phagocytic cells. bone marrow-derived macrophages were used. A significant increase in the ratio of pro-inflammatory (%CD80+CD86+ in F4/80+) to antiinflammatory M\$\psi\$s (%CD163\pm20206\pm in F4/80\pm) in the PES MPtreated group was observed as compared to monomers and the untreated control. The ratio of pro-inflammatory to anti-inflammatory Mos, treated with PES MPs along with CB-839, was also significantly higher than any other treatment group (Supplementary Fig. S19). Overall, these data indicate that intracellular delivery of a metabolite succinate using PES MPs was able to induce a pro-inflammatory phenotype in phagocytes. Although PES MPs [66] demonstrate that they can activate phagocytes effectively, without adjuvants, nanoparticles generated from PES may further increase this activation, due to faster degradation kinetics.

To determine PES MPs' ability to generate an anti-tumor immune response in vivo, a highly aggressive and large established murine melanoma (B16F10) model was utilized (Fig. 4a,b). CB-839 was also used as it can metabolically impair cancer cells. [67,68] Indeed, it was determined that CB-839 was effective in preventing proliferation of B16F10 cancer cells with an IC50 of 0.743 µM in vitro (Supplementary Fig. S20). Also, the basal respiration of B16F10 cells significantly decreased upon incubation with TRP2(coated)PES MPs (Supplementary Fig. S21); however, no significant changes in glycolysis were observed due to PES MPs. After in vivo treatment of formulations in mice with established B16F10 tumors, no significant changes in mice weight (Supplementary Fig. S22) were observed. Moreover, the effect of PES MPs on liver health in these mice was studied by measuring the serum's alanine transaminase (ALT) levels. There were no significant differences observed between untreated mice and those treated with soluble succinate, PES MPs, and TRP2(tyrosine related protein 2, antigen for melanoma [69,70]) (coated)PES MPs (Supplementary Fig. S23). To test whether PES MPs change the succinate levels in the serum, a succinate assay kit was used, and there were no significant differences observed in untreated mice and those treated with soluble succinate, PES MPs, and TRP2(coated)PES MPs as compared to naïve young mice (Supplementary Fig. S24). These data suggest that PES MPs might act locally and might not have a significant systemic effect.

Next, mouse survival was measured after treatment with different formulations. Mice treated with the vehicle alone ($1 \times PBS$) survived for only 22 days. Similarly, mice treated with other controls, such as soluble

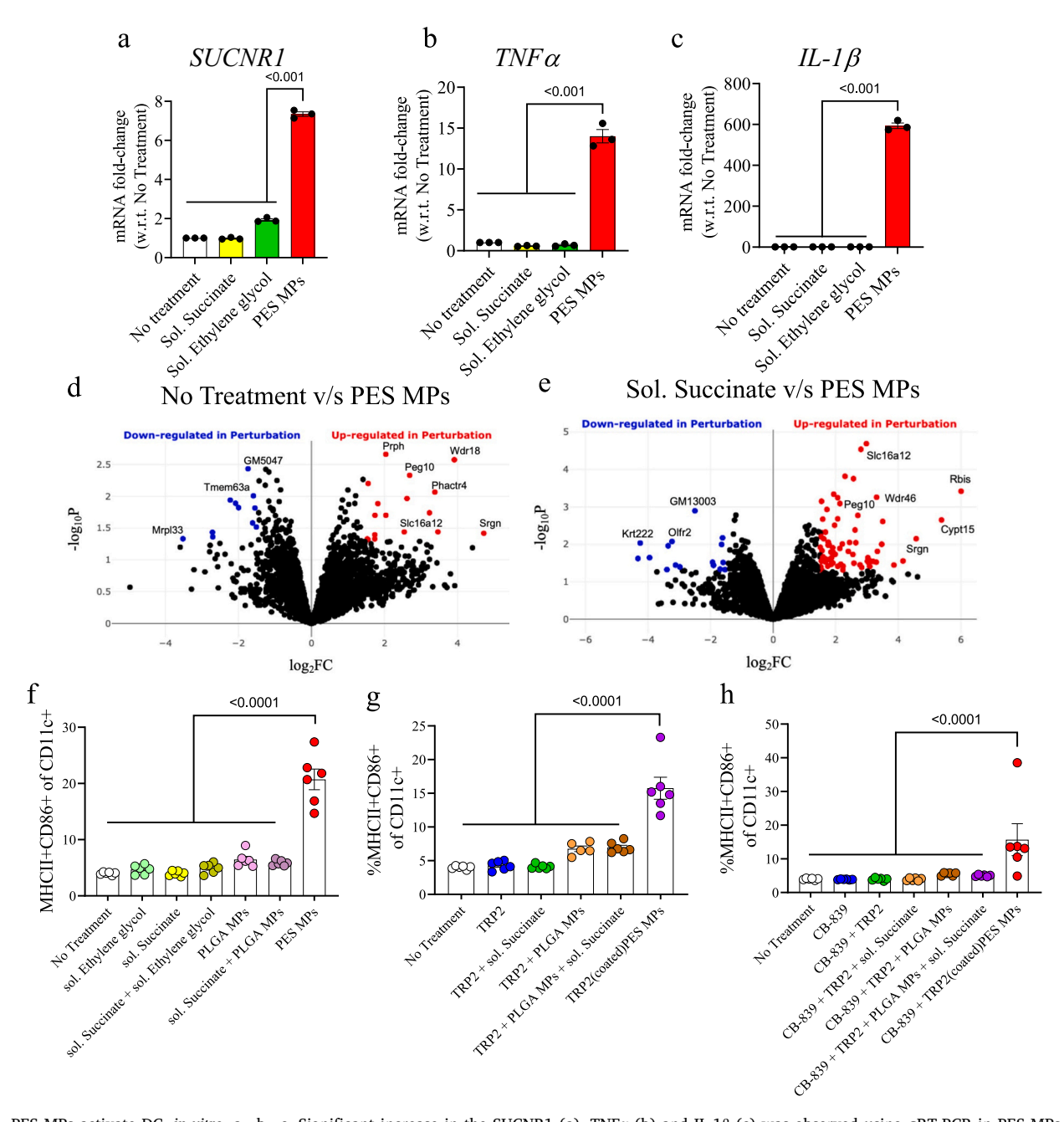


Fig. 3. PES MPs activate DC, *in vitro*. a., b., c. Significant increase in the SUCNR1 (a), TNF α (b) and IL-1 β (c) was observed using qRT-PCR in PES MPs DCs as compared to other treatment groups (n=3; One-way ANOVA, Tukey-test). d., e. RNA-seq indicated a pro-inflammatory phenotype of DCs treated with PES MPs as compared to untreated (n=3; two-tailed unpaired Student's *t*-test, FC = fold change; P = *p*-value). (d) and soluble succinate treated (e) groups (n=3). f., g., h. There was a significant increase in activation phenotype of DCs when treated with PES MPs and TRP2(coated)PES MPs as compared to other treatment groups (n=6; One-way ANOVA Tukey test). Data depicted as average \pm std. error.

succinate and soluble TRP2, survived until day 24 and day 26, respectively. Moreover, 60% of the mice treated with PES MPs survived until day 31. Additionally, mice treated with TRP2(coated)PES MPs survived until day 36, suggesting that TRP2(coated)PES MPs alone can increase survival in tumor-bearing mice (Fig. 4b,d).

Next, the cooperation between CB-839 and succinate delivery was tested *in vivo*. To test if the encapsulated *versus* coated TRP2 lead to differential responses, these two formulations were generated. It was observed that TRP2(coated)PES MPs had $76 \pm 4~\mu g$ of TRP2 per mg of PES MPs, on the other hand TRP2(encap)PES MPs had $77 \pm 6~\mu g$ of TRP2 per mg of PES MPs. Systemic delivery of CB-839 and subcutaneous (s.c.) treatment with PES MPs encapsulated with TRP2 led to 100% survival up to day 22, 40% survival up to day 32, and eventually 20% survival up

to day 45, which suggests that simultaneous succinate delivery, along with GLS1 inhibition, can further prolong mouse survival (Fig. 4c,d). Controls of CB-839 only and CB-839 + soluble TRP2 led to survival until day 27, suggesting that GLS1 inhibition alone and antigens alone can have a modest effect on survival. To test the effect of increased amounts of TRP2 for DC antigen processing and presentation on survival and tumor growth, PES MPs coated with TRP2 were used (Supplementary Fig. S25). Treating the mice with CB-839 and PES MPs coated with TRP2 led to 100% survival up to day 35, 60% up to day 41, and eventually no survival after day 60 (Fig. 4c,d). In fact, increasing the levels of TRP2 while injecting with PES MPs may lead to even stronger responses and longer survival in mice. Immunofluorescent images of end-stage tumors from mice treated with different treatment groups indicated a

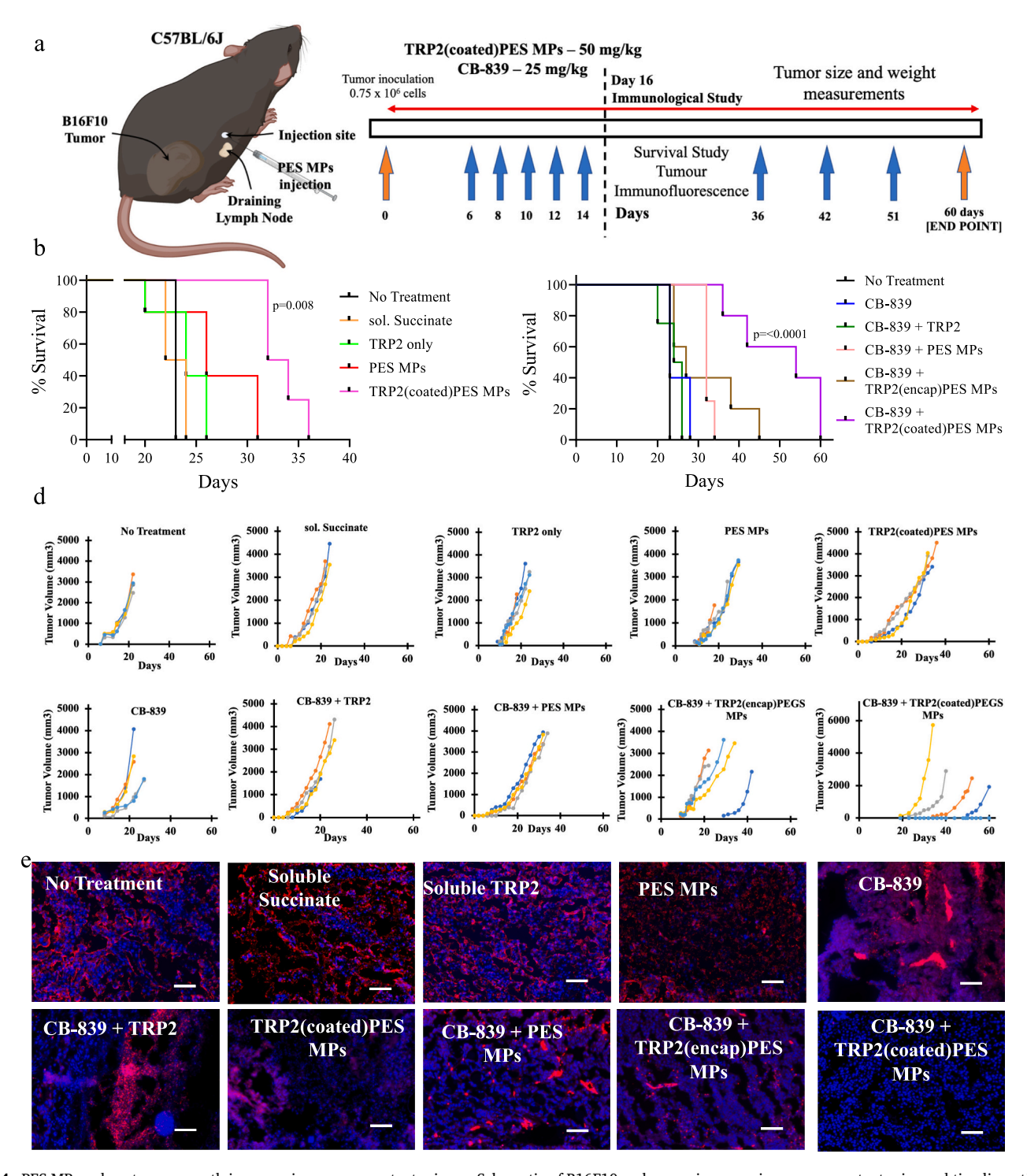


Fig. 4. PES MPs reduce tumor growth in young immunocompetent mice. a. Schematic of B16F10 melanoma in young immunocompetent mice and timeline utilized for this study. b. Kaplan Meir curve indicating higher survival rate in mice treated with TRP2(coated)PES MPs as compared to other treatment groups (n = 5; Logrank Mantel Cox test). c. Kaplan Meir curve indicating higher survival rate in mice treated with CB-839 + TRP2(coated)PES MPs as compared to other treatment groups (n = 5; Logrank Mantel Cox test). d. Tumor volume data for individual mouse for all treatment groups. e. Representative immunofluorescence images of tumors at end point of mouse survival indicate lower TRP2 expressing cells in TRP2(coated)PES MPs group as compared to other treatment groups. Scale bar = 100 μ m. Red = TRP2, Blue = nuclei. (For interpretation of the references to colour in this figure legend, the reader is referred to the web version of this article.)

significantly lower population of cells expressing TRP2, suggesting the potency of treatment with TRP2(coated)PES MPs (Fig. 4e, Supplementary Fig. S26, S27).

To analyze whether the tumor responses observed due to PES MPs were indeed associated with DC phenotype *in vivo*, mice were sacrificed on day 16 post-tumor induction, and lymph nodes and tumors were

harvested for analysis using RNA sequencing and flow cytometry. Tumors harvested on day 16 were significantly smaller in mice treated with PES MPs coated with TRP2 as compared to other treatment groups (Supplementary Fig. S28). DCs were isolated from draining lymph nodes using $\mbox{CD11c}^+$ magnetic beads from untreated and PES MP-treated mice, and bulk RNA-seq was performed to study their RNA profile (Fig. 5a). A

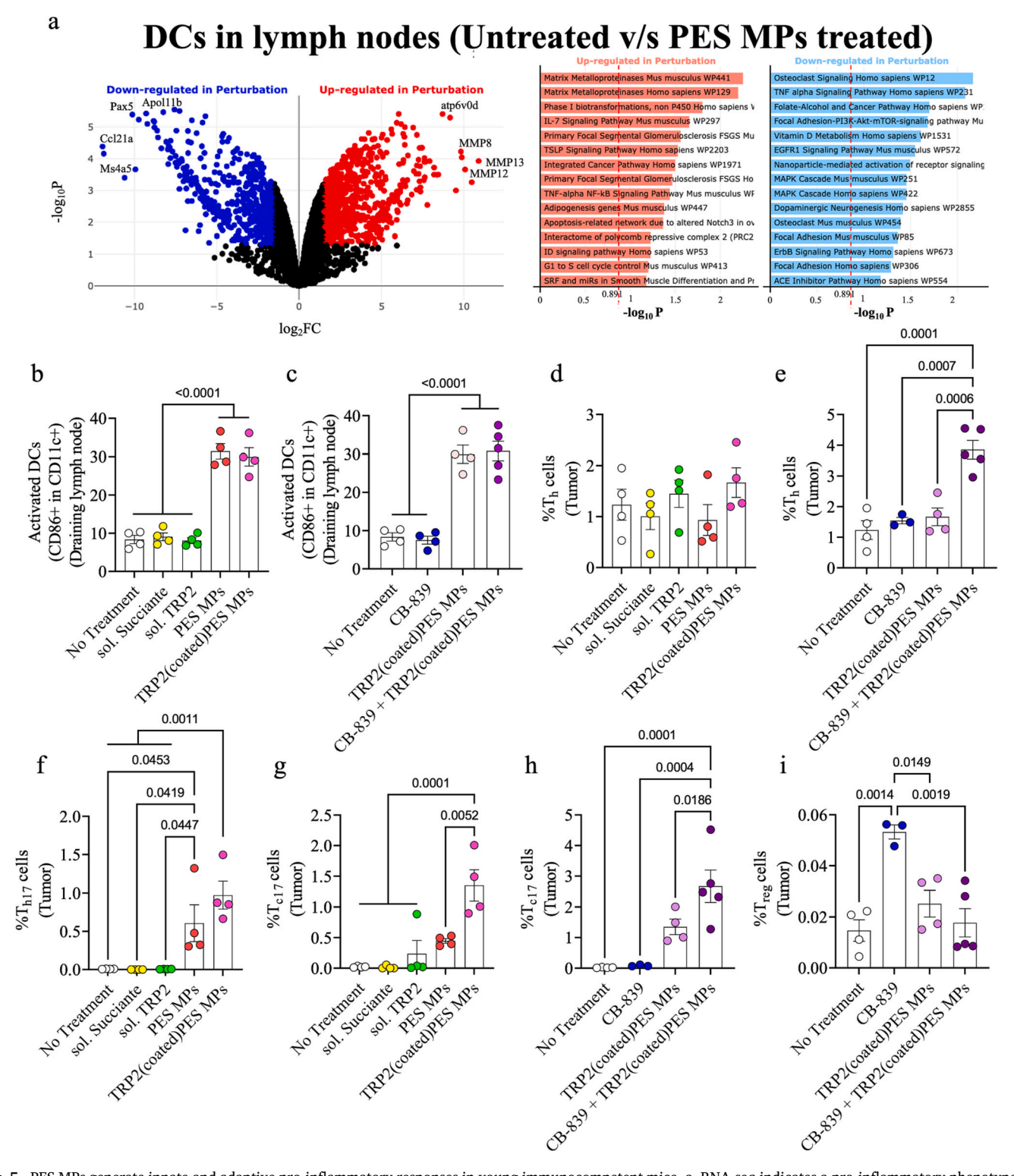


Fig. 5. PES MPs generate innate and adaptive pro-inflammatory responses in young immunocompetent mice. a. RNA-seq indicates a pro-inflammatory phenotype of DCs isolated from draining lymph nodes of mice treated with PES MPs and PBS (untreated) (n=3; two-tailed unpaired Student's t-test, FC = fold change; P = p-value; red line indicates p=0.05). b. Mice treated with PES MPs and TRP2(coated)PES MPs had significantly higher frequency of activated DCs (shown as %CD86 in CD11c+) in the draining lymph node as compared to other controls (One-way ANOVA; Tukey test). c. Mice treated with CB839 + TRP2(coated)PES MPs had significantly higher activated DCs in the draining lymph node as compared to other controls (One-way ANOVA; Tukey test). d., e. Significant increase as observed in percentage of Th cells (%CD4+ in all cells) in the tumors of mice treated with TRP2(coated)PES MPs and CB839 + TRP2(coated)PES MPs as compared to other treatment groups, respectively (One-way ANOVA; Tukey test). f., g., h. Significant increase in Th17 (%RORgt+ in CD4+ cells) and Tc17 (%RORgt+ in CD8+ cells) cells was observed in the tumors of TRP2(coated)PES MP-treated as well as CB-839 + TRP2(coated)PES MP-treated mice as compared to other treatment groups (One-way ANOVA; Tukey test). i, Significant changes in Tregs (%CD25 + Foxp3+ in CD4+) were observed in tumors of CB-839 + TRP2(coated)PES MPs treated mice as compared to other treatment groups (One-way ANOVA; Tukey test). Data depicted as average \pm std. error. (For interpretation of the references to colour in this figure legend, the reader is referred to the web version of this article.)

significant increase in the matrix metalloproteinases pathways (MMPs) was observed, attributed to upregulation of MMP8, MMP12, and MMP13 in the DCs isolated from PES MP-treated lymph nodes as compared to untreated lymph nodes. Studies suggest that these MMPs play an essential role in cell migration, proliferation, and differentiation. Specifically, MMP13 in DCs has been found to play a major role in immunostimulatory function through MHC molecules. One such study showed that inhibition of MMP13 not only downregulated the CD11c expression on DCs but also affected their ability to activate cytotoxic T cells. [70] Next, a significant increase (~4-fold) in the percentage of activated DCs in the draining lymph nodes of mice treated with PES MPs and TRP2 (coated)PES MPs was observed with flow cytometry as compared to other controls, which suggests that PES MPs were able to activate DCs in vivo (Fig. 5b). Similarly, a significant increase (~3-fold) in the percentage of activated DCs was observed in CB-839 + PES MP-treated and CB-839 + TRP2(coated)PES MP-treated mice as compared to controls, indicating that PES MPs, in vivo, are able to activate DCs (Fig. 5c). Since, microparticles get entrapped in the interstitial matrix at the injection stie and nanoparticles are required for draining into the lymph nodes, it is not expected that the PES MPs might be captured by DCs and then trafficked to the lymph nodes. [71,72] Also activation of DCs is essential for melanoma tumor responses in vivo, [73,74] and PES MPs showed a higher activation of DCs in the lymph nodes, PES MPs might be responsible for developing these anti-tumor responses. In vitro the activation of the DCs was skewed towards activation by intracellular delivery of succinate, as evidenced by increased activation due to PES MPs as compared to soluble succinate. However, in vivo due to sustained release of succinate from the PES MPs, it is expected that the cells will be exposed to succinate both in an extracellular and intracellular manner. Nonetheless, given the in vitro data it is expected that the intracellular delivery of PES MPs to the DCs might be responsible for causing the activation of DCs in vivo as well.

Mice treated with different formulations and sacrificed on day 16 were also analyzed for the T-cell phenotype (Figs. 5d-i, Supplementary Fig. S29, S30). For increasing the accuracy of counting the T cells in the tumor, a CD45, the viability dye or a CD3 can be included in analyses, since other immune cells such as DCs can express these markers as well. Significant differences were observed in helper T cells (Th cells) in tumors found in in untreated mice as well as those treated with soluble succinate, TRP2, PES MPs, and TRP2(coated)PES MPs (Fig. 5d,f,g; Supplementary Fig. S30). There was a significant increase in Th cells in CB-839 + TRP2(coated)PES MP-treated mice as compared to untreated, CB-839-treated and TRP2(coated)PES MP-treated mice (Supplementary Fig. S30, Fig. 5d). Similarly, there was a significant increase in the proliferating Th cells in tumors of mice treated with CB-839 + TRP2 (coated)PES MPs as compared to controls (Supplementary Fig. S30). Interestingly, there was a significant increase in Th17 cells in mice treated with PES MPs and TRP2(coated)PES MPs as compared to untreated mice and those treated with soluble succinate or soluble TRP2 (Fig. 5f). Furthermore, there were significant changes observed in other helper T cells in tumors treated with CB-839 + TRP2(coated)PES MPs as compared to controls (Supplementary Fig. S30). Moreover, Tc17 cells significantly increased (\sim 2.5-fold) in mice treated with CB-839 + PES MPs as compared to controls (Fig. 5i). Although there were no significant changes observed in regulatory T cells (Tregs) in the tumors of untreated mice or mice treated with soluble succinate, TRP2, PES MPs, or TRP2(coated)PES MPs (Supplementary Fig. S30), there was a significant decrease in the Tregs in CB-839 + TRP2(coated)PES MPs when compared to CB-839 alone (Fig. 5i). Also, TRP2(coated)PES MPs were able to significantly upregulate Tc1 (%Tbet+ in CD8+) cells as compared to soluble succinate and no treatment control. Moreover, there was no significant differences found between CB-839 + TRP2 (coated)PES MPs treated mice as compared to TRP2(coated)PES MPs in Tc1 frequency in tumor (Supplementary Fig. S31). This data suggests that TRP2(coated)PES MPs by themselves are able to increase the frequency of Tc1 in the tumor, which will be further investigated in the

future studies. Overall, these data suggest that the decrease in tumor sizes observed in mice treated with TRP2(coated)PES MPs was driven by an increase in pro-inflammatory Tc17 and Tc1 cellular phenotype. In the tumor microenvironment due to paucity of nutrients and factors released by cancer cells, T cells can undergo exhaustion [75,76]. Functional activation of these T cells has been achieved using therapies that modulate metabolic pathways in these cells [77,78]. The functional effectiveness of these T cells can be studied by the cytokine production from these cells [79–81]. These will be the focus of future studies. Although, flow cytometry was utilized to understand T cell and DC functions in the tumor microenvironment, a direct visualization of immune cell infiltration will also provide confirmation of the flow data. Immunohistochemistry (IHC) experiments and hematoxylin and eosin were not performed in this project, and will be the focus of future studies.

In conclusion, this study demonstrates that succinate-based polymeric activate DCs by modifying the TCA cycle, glutamine and glutamate metabolism; modulating SUCNR1 and HIF-1alpha; upregulating the TSLP and EGF/EGFR- and EGFR1-signaling pathways while downregulating TGF-beta pathway. Hence, these PES MPs. MPs act as alarmins by modulating the immunometabolism of DCs to generate robust pro-inflammatory responses. Moreover, these biomaterials generate a robust anti-tumor response, which is necessary for melanoma treatment in immunocompetent young mice, as well as in aging immuno-defective mice. Overall, this approach can provide a versatile platform for the development of immunotherapeutic strategies for cancer treatment.

3. Methods

3.1. Polymer synthesis

Succinic acid and alkane diol (namely, 1,4-butanediol, 1,6-hexanediol, 1,8-octanediol or 1,10-decanediol) were mixed at equimolar ratio in a round-bottom flask. This mixture was stirred at 90 $^{\circ}$ C for 3 h under vacuum. The polymer thus generated was precipitated in methanol solution. A rotary evaporator was used to evaporate the remaining methanol, and the polymers were dried under vacuum at room temperature for 48 h. Size exclusion chromatography (SEC) was used to determine the polymers' molecular weight.

3.2. ¹HNMR

To determine the polymer structure, 1 H NMR spectroscopy was performed using a Varian 500 MHz spectrometer. For this characterization, 20 mg of dried polymer was dissolved in 0.7 g deuterated chloroform and Dimethyl sulfoxide (CDCl₃ and DMSO- d_6). Chemical shifts are given in ppm downfield from tetramethyl silane (TMS).

3.3. Molecular weight calculation

Size exclusion chromatography (SEC) was carried out using a Waters Alliance e2695 HPLC system interfaced to a light-scattering detector (miniDAWN TREOS) and an Optilab T-rEX differential refractive index (dRI) detector to determine the polymers' molecular weight. The mobile phase was THF Optima (inhibitor-free) at a flow rate of 1.0 mL/min. The elution times of the polymer samples are compared to a universal calibration curve prepared from 6 low dispersity polystyrene standards of 5 kDa, 10 kDa, 30 kDa, 100 kDa, 200 kDa and 500 kDa molecular weights (Agilent technologies and Pressure chemical company). The molecular weight analysis was performed using Astra v6.1 software. The polymer solutions were prepared by dissolving the samples in THF, which had been passed through an M. Braun SPS-800 solvent purification system at a concentration of $\sim\!2.0$ mg/mL and then passed through a 0.45 μm filter.

3.4. Microparticle generation

Succinate-based polymers were used to generate microparticles (MPs) using a standard oil-water emulsion method. Specifically, 50 mg of the polymer was dissolved in 1 mL of dichloromethane (DCM, Fischer Scientific, Pittsburgh, PA). In order to generate TRP2(encapsulated)PES MPs, 150 µg of TRP2 was dissolved along with 50 mg of the polymer in 1 mL of dichloromethane. The solution was then added to 10 mL of 2% polyvinyl alcohol (PVA) solution in 18.2 W nanopure water and homogenized at either 10,000 rpm or 30,000 rpm (for >20 μ m particles) using a handheld homogenizer (DREMEL 8220) for 2 min, depending upon the required size. The resulting emulsion was added to a continuously stirred 50 mL solution of 1% PVA set at 400 rpm for up to 2 h to allow for DCM evaporation. Subsequently, the particles were washed 3 times by centrifuging at 2000 Gs for 5 min, removing supernatant and resuspending in nanopure water each time. The microparticles were then lyophilized and stored at $-20~^{\circ}\text{C}$ and used for subsequent experiments. MPs were generated using the same method for all synthesized

In order to generate TRP2(coated)PES MPs, 10 mg of the lyophilized PES MPs were dissolved in 1 mL of 1× PBS along with 1 mg of TRP2. The mixture was thoroughly vortexed for 30 s and subsequently washed 3 times by centrifuging at 2000 Gs for 5 min, removing supernatant and resuspending in nanopure water each time. Finally, the particles were suspended in 1× PBS (10 mg/mL) and stored at $-20\ ^{\circ}\text{C}$ and used for subsequent experiments.

3.5. Particle size determination

The size of the succinate-based microparticles was quantified using dynamic light scattering (Zetasizer Nano ZS, Cambridge, UK). Additionally, microparticles were imaged using scanning electron microscopy (SEM) XL30 Environmental FEG - FEI at Erying Materials Center at Arizona State University.

3.6. Release kinetics

Release kinetics of succinate from microparticles was determined by incubating 1 mg of the microparticle in 1 mL of phosphate buffered saline (PBS) at pH 7.4, in triplicates. The samples were placed on a rotator at 37 °C throughout the course of 30 days. At each time point, the samples were centrifuged at 2000 X Gs for 5 mins. Post centrifugation, 800 µL of the supernatant was removed and stored in a 1.7 mL microcentrifuge tubes at -20 °C for further use. Finally, $1 \times$ PBS buffer (800 μL) was added to the original samples, and the process was continued for each time point. The amount of metabolite released was then determined by developing a new method in high-performance liquid chromatography (HPLC, Agilent Technologies, Santa Clara, Specifically, the mobile phase of 0.02 M H₂SO₄ in water was used. A 50 μL of injection volume was utilized in a Hi-Plex H, 7.7 \times 300 mm, 8 μm column. The flow rate of 1.2 mL/min was utilized and the absorbance was determined using a UV detector at 210 nm. The area under the curve was determined using the ChemStation analysis software as per manufacturer's directions.

For release kinetics of TRP2 from MPs, 5 mg of MPs were incubating in 1 mL of PBS at pH 7.4, in triplicates. The samples were placed on a rotator at 37 $^{\circ}\text{C}$ throughout the course of 24 h. The peptide concentration was determined using nanodrop, by first generating a standard curve of TRP2 peptide from known concentration. The unknown concentration of TRP2 in the solution was determined by pipetting 2 μL of the sample and measuring the absorbance at 280 nm.

3.7. Endotoxin measurement assay

ToxinSensor™ Chromogenic LAL Endotoxin Assay Kit (GenScript) was used to measure endotoxin levels in the synthesized PES MPs.

3.8. Dendritic cell isolation and culture

Bone marrow-derived Dendritic Cells (BMDCs) were generated from 6 to 8-week-old female C57BL/6j mice in compliance with the protocol approved by Arizona State University (protocol number 19-1688R) using a modified 10-day protocol. Femur and tibia from mice were isolated and kept in wash media (DMEM/F-12 (1:1) with L-glutamine (VWR, Radnor, PA), 10% fetal bovine serum (Atlanta Biologics, Flowery Branch, GA) and 1% penicillin-streptomycin (VWR, Radnor, PA). The ends of the bones were trimmed, and bone marrow was flushed out with 5 mL wash media and made into a homogenous suspension. Red blood cells (RBC) were lysed by centrifuging the suspension and incubating in 3 mL of $1\times$ RBC lysis buffer for 5 mins on ice. The cell suspension was centrifuged and washed with 7 mL wash media before resuspension in DC media DMEM/F-12 with L-glutamine (VWR, Radnor, PA), composed of 10% fetal bovine serum, 1% sodium pyruvate (VWR, Radnor, PA), 1% non-essential amino acids (VWR, Radnor, PA), 1% penicillin-streptomycin (VWR, Radnor, PA), and 20 ng/mL GM-CSF (VWR, Radnor, PA)). The cells were later seeded in a tissue culture treated T-75 flask (Day 0). On day 2, floating cells were collected, centrifuged, and resuspended in fresh media, respectively, and seeded on ultra-low attachment plates for 7 additional days. The media was changed every day until day 9. On day 9, cells from the ultra-low attachment plates were resuspended and 0.1×10^6 cells/well were seeded on suitable tissue culture plates for the desired experiments for 1 more day (until day 10) before treatment. Cells in the tissue culture plates were used for further experiments/treatment on day 10. The purity, immaturity and yield of DCs and M\psi was verified via immunofluorescence staining and flow cytometry. DCs and M\psis were isolated from at least 3 separate mice for each type of experiment.

3.9. Confocal microscopy

On day 10, 0.1 million cells were seeded on a glass slide within 24 well plates and were incubated for 24 h in 37 °C. The cells were then treated with fluorescently labelled FITC-PES MPs. The nucleus and cytoplasm were stained with DAPI and rhodamine-phalloidin, respectively. Samples were imaged with a Nikon C2 laser scanning confocal microscope using a 60×, oil-immersion lens with numerical aperture of 1.4. DAPI, and fluorescently labelled rhodamine-PES MPs were excited with 405 nm and 561 nm lasers respectively, coupled with appropriate blue and red channel-emission detection. Image dimensions were 1024 \times 1024 pixels scanned with a digital zoom of 2×. Z-stacks were created in the same manner, with a step size of 0.25 µm between optical slices. Cells treated with FITC-PES MPs MPs and untreated cells were used as negative imaging controls to identify the signal of interest. Laser intensity and detector gain were adjusted to eliminate background or autofluorescence and avoid pixel saturation. Elements, a Nikon software, was used to adjust the intensity scale, create orthogonal views, and convert images to 8-bit TIFF format.

3.10. GC-MS metabolic flux assay

Dried samples from the metabolite extraction were incubated at 60 °C for 90 min with a solution of 40 μL of 20 mg/mL O-methylhydroxylamine hydrocholoride in pyridine. Then 70 μL of MTBSTFA was added and incubated again at 60 °C but for 30 min. Next, an Agilent 7820 GC-5977 MSD system (Agilent Technologies, Inc., Santa Clara, CA, USA) was used for GC–MS spectral acquisition. The GC–MS was run in splitless mode, with a carrier gas of helium (purity >99.999%) and the use of 1 μL of derivatized sample for injection. After, a Zorbax DB5-MS + 10 m Duragard Capillary Column (30 m \times 250 μm \times 0.25 μm) was used to obtain chromatographic separation. The column's temperature was kept at 60 °C for 1 min before being increased at a rate of 10 °C per minute until the temperature reached 325 °C, which was kept at for 10 min. The mass spectral signals were recorded in full-scan mode, using

electron ionization (El, 70 eV) with the mass range at 50–600 Da. The collected raw GC–MS data was analyzed using Agilent MassHunter software (Version B.09.00) in a targeted way to monitor compounds. Each sample's isotopomer distributions (MIDs) were calculated by integrating metabolite ion fragments, and the natural abundance of isotopes was corrected with IsoCor software.

3.11. Extracellular flux assays

Oxidation consumption rate (OCR) was measured using Seahorse Extracellular Flux XF-96) analyser (Seahorse Bioscience, North Billerica, MA. Briefly, 200,000 cells/well were seeded in Seahorse XF-96 plates and cultured. Cells were treated with 50 $\mu g/well$ PES, 30 nM CB-839, 10 $\mu g/mL$ LPS or no treatment control. After 24 h, for OCR, media was changed to unbuffered DMEM containing 2 mM glutamine, 1 mM pyruvate, and 10 mM glucose following sequential injections of oligomycin (2 mM), 7 Carbonyl cyanide-4 (trifluoromethoxy) phenylhydrazone (FCCP) (1 mM), and antimycin/rotenone (1 mM). The OCR after the injection of oligomycin was a measure of ATP-linked respiration and the OCR after the injection of FCCP represented maximal respiratory capacity. Basal respiration was quantified by measuring OCR prior to the injection of oligomycin. All samples were analyzed with 6 technical replicates.

$3.12.\ LC$ -MS/MS metabolomics studies to determine levels of intracellular metabolites

Bone marrow derived DCs from C57BL/6 J were cultured in 6 well plates at 1 million cells per well. PES microparticles were added at 50 $\mu g/well$ and no treatment was used as a control. After 24 h of culture, the supernatant was removed, and the cells were gently rinsed with 2 mL of 37 °C PBS. Next, immediately, 1 mL of 80:20 methanol:H₂O (-80 °C) into the plates, and the plates were then placed on dry ice to quench metabolism and perform extraction. After 30 min of incubation on dry ice, the cells were scraped with a cell scraper (VWR, Radnor, PA) and transferred into centrifuge tubes. The tubes were then spun at 16,000 rpm for 5 min at 4 °C (Eppendorf, Hauppauge, NY, USA). The soluble extract was removed into a vial and completely dried. The pellets were utilized to measure the total protein using Nanodrop 2000 (Thermo-Fisher Scientific, Waltham, MA, USA).

The LC-MS/MS method was performed according to previous reported protocols. Agilent 1290 UPLC-6490 QQQ-MS (Santa Clara, CA) system was used to perform LC-MS/MS. Briefly, 10 µL of the processed samples were injected twice, for analysis using negative ionization mode and a total of $4 \mu L$ of the processed sample for analysis using positive ionization mode. Both chromatographic separations were performed in hydrophilic interaction chromatography (HILIC) mode on a Waters XBridge BEH Amide column (150 \times 2.1 mm, 2.5 μ m particle size, Waters Corporation, Milford, MA). A 0.3 mL/min flowrate was used, along with temperatures for the auto-sampler set at 40 °C and the column compartment at 40 °C, respectively. The mobile phase was composed of Solvents A - 10 mM ammonium acetate, 10 mM ammonium hydroxide in 95% $H_2O/5\%$ ACN and Solvent B - 10 mM ammonium acetate, 10 mM ammonium hydroxide in 95% acetonitrile (ACN)/5% H₂O. After the initial 1 min isocratic elution of 90% B, the percentage of Solvent B decreased to 40% at t=11 min. The composition of Solvent B was maintained at 40% for 4 min (t = 15 min), following which the percentage of B gradually went back to 90% to prepare for the next injection.

The mass spectrometer is equipped with an electrospray ionization (ESI) source. Targeted data acquisition was performed in multiple-reaction-monitoring (MRM) mode. A total of $\sim\!320$ MRM transitions in negative and positive modes were observed. The whole LC-MS system was controlled by Agilent Masshunter Workstation software (Santa Clara, CA); extracted MRM peaks were integrated using Agilent Mass-Hunter Quantitative Data Analysis (Santa Clara, CA).

3.13. RNA isolation and aRT-PCR

A PureLink RNA Mini Kit (12183018A, 12183025) was used to isolate RNA from the treated DCs, 24 h post treatment. Subsequently, the isolated RNA was used for qRT-PCR analysis, which was performed with TaqMan \circledR Gene Expression Assay, according to manufacturer instructions.

	GENE	COMPANY	Assay ID
1	Primer for Actinb (Actb)	ThermoFisher Scientific	Mm02619580_g1
2	Primer for BCL3	ThermoFisher Scientific	Mm00504306_m1
3	Primer for Glut1 (Slc2a1)	ThermoFisher Scientific	Mm00441480_m1
4	Primer for HIF1a	ThermoFisher Scientific	Mm00468869_m1
5	Primer for IL-1beta (IL1b)	ThermoFisher Scientific	Mm99999061_mH
6	Primer for NFkB (Nkap)	ThermoFisher Scientific	Mm00482418_m1
7	Primer for NLRP3	ThermoFisher Scientific	Mm04210224_m1
8	Primer for PPARG	ThermoFisher Scientific	Mm00440940_m1
9	Primer for SUCNR1	ThermoFisher Scientific	Mm00519024_m1
10	Primer for TNF	ThermoFisher Scientific	Mm00443258_m1

3.14. RNA-seq

Using KAPA's mRNA HyperPrep Kit (KAPA KK8580), mRNA sequencing libraries were generated from total RNA. Magnetic oligo-dT beads captured mRNA, which was then sheared to approximately 300-350 bp using heat and magnesium. The 1st strand of the mRNA fragments was reverse transcribed using random priming. The 2nd strand was generated with incorporated dUTP molecules to allow for strand-specificity. Illumina-compatible adapters with unique indexes (IDT #00989130v2) were ligated on each sample individually. The adapter ligated molecules were amplified for 10 cycles with Kapa's HIFI enzyme (KAPA KK2502). Fragment size was verified to be 450-500 bp on an Agilent Tapestation and quantified with a Qubit before multiplex pooling and sequencing a 2 \times 150 flow cell on the Illumina Nova-Seq6000 platform at the University of Colorado Anschutz Medical Campus Genomics Core facility.

3.15. MTT assay

Cell proliferation was determined using MTT reagent. Specifically, B16F10 cells were cultured in DMEM/F-12 (1:1) with L-glutamine supplemented with 10% fetal bovine serum and 1% penicillin-streptomycin. Briefly, cells were seeded in flat-bottomed 96-well plates (10,000 cells per well) overnight. On the day of the treatment, CB-839 with varying concentrations were added to B16F10, respectively. Equal volume of DMEM/F-12 (1:1) was added in the no-treatment group as negative control. For positive control (all dead cells), media from wells was aspirated and methanol was added to the wells for 15 min, ensuring the death of all cells in the well, following which methanol was siphoned off and an adequate amount of media was re-added to the wells. After 48 h, $10~\mu L$ of the MTT solution was added to all wells, and the plates were placed at 37 °C for 3 h in the dark. Supernatants from all the wells were aspirated and 50 µL of DMSO:Methanol (1:1) was added to all wells following which the plates were placed in the dark at 37 °C ensuring delicate stirring of the plates. The number of viable cells was determined by measuring absorbance at 570 nm with a reference wavelength of 670 nm using a plate reader (Speedmax M2e, Sunnyvale, CA).

3.16. Flow cytometry

Flow cytometry (FACS) staining buffer was prepared by generating 0.1% bovine serum albumin (VWR, Radnor, PA), 2 mM Na₂EDTA (VWR, Radnor, PA) and 0.01% NaN₃ (VWR, Radnor, PA). Live/dead staining was performed using fixable dye eF780 (ThermoFisher Scientific, Waltham, MA, USA). All antibodies required for staining were purchased and used as is (BD biosciences, Tonbo Biosciences, BioLegend, Thermo

Scientific, Invitrogen). Flow cytometry was performed by following the manufacturer's recommendation and guidelines set by ASU flow cytometry core using Attune NXT Flow cytometer (ThermoFisher Scientific, Waltham, MA, USA). The reagents and antibodies used in the study are as follows:

-	are as follows.				
	Target	Fluorophore	Company	Catalog #	Clone
1	CD4	PE	BD	12–0041- 82	GK1.5
2	CD8	APC-R700	BD	564,983	53-6.7
3	CD25	PECy7	BD	552,880	PC61
4	CD11c	PE	BioLegend	117,308	N418
5	CD86	SB600	Thermo	63–0862- 82	GL1
6	CD80	PE-Cy5	Invitrogen	15–0801- 82	16-10A1
7	MHCII	APC	BioLegend	107,614	M5/ 114.15.2
8	Tbet	BV785	BioLegend	644,835	4B10
9	FoxP3	eF450	Invitrogen	48–5773- 82	FJK-16 s
10	RORgT	BV650	BD	564,722	Q31-378
11	Ki67	FITC	Invitrogen	11–5698- 82	SolA15
12	GATA3	BV711	BD	565,449	L50-823
13	CD16/CD32:Fc Block	NA	Tonbo	70–0161- M001	2.4G2
14	F4/80	BV702	Invitrogen	67–4801- 80	BM8
15	Comp beads	NA	Invitrogen	01–2222- 42	NA
16	Cell stimulation cocktail (with golgi stop) Cell activating	NA	Tonbo	TNB- 4975- UL100	NA
17	cocktail (w/o brefeldin A)	NA	BioLegend	423,301	NA
18	L/D	eF780	NA	NA	NA
19	IL12	V450	BD	561,456	C15.6
20	IFNY	PE	Tonbo	50–7311- U100	XMG1.2
21	IL10	PE/DAZZLE	BioLegend	505,034	JES5- 16E3
22	TNFa	BV510	BD	563,386	MP6- XT22
23	Golgi Stop	NA	BD	554,724	NA
24	Golgi Plug	NA	BD	555,029	NA
25	CD11b	FITC	Tonbo	35-0112- U500	M1/70
30	Foxp3 / Transcription Factor Staining Buffer Set (Fix/ Perm concentrate and dilutent, and 10× perm buffer)	NA	ThermoFisher	00–5523- 00	NA

3.17. Intracellular cytokine quantification of IL-10, IL-12p70, and TNF α

Post 16 h of treatment, golgi stop (BD Biosciences, San Jose, CA) and golgi plug (BD Biosciences, San Jose, CA) were added to each treatment well. The plates were then incubated for a further 5 h at 37 °C. Cells were then surface stained with CD11c and intracellularly stained for cytokines (IL-10, IL-12p70, TNF α). All reagents and incubations were kept at 4 °C during the staining.

3.18. ELISA

A DuoSet ELISA development system (DY410–05) was used to measure $TNF\alpha$ from the extracellular supernatant of treated DCs. Final measurements were taken using plate reader (Speedmax M2e) as per the manufacturer's instructions.

3.19. Tumor Induction and treatment for young mouse model

Female C57BL/6j mice, 6-8 weeks, were obtained from Jackson Laboratory (Bar Harbor, ME). Experiments were performed in compliance with IACUC guidelines of ASU (protocol no. 19-1688R). Melanoma cell line, B16F10, were cultured at 37 °C in a 5% CO2 atmosphere in DMEM/F12 with L-glutamine, 10% fetal bovine serum, 1% penicillin-streptomycin (culture media). For inoculation, cells were removed from flasks using a trypsin solution, centrifuged, and resuspended in 5 mL culture media. Trypan blue exclusion was used to determine cell viability. Furthermore, cells were counted and resuspended in sterile PBS to obtain a solution of 7.5×10^6 cells/1 mL. Finally, mice were s.c. injected with 0.75×10^6 cells/mouse (100 μL) into the right thigh. All mice were randomized and divided into 10 mice/group before inoculation with tumor cells. Mice were treated intraperitoneally on day 6 with 25 mg/kg CB-839 (unless otherwise mentioned) and 1 mg of microparticles s.c. (0.5 mg on top of the general thigh area on either side) three times a week. Mice weight and tumor growth were measured and recorded every other day. Tumor growth was measured using a digital caliper and calculated as (longest length*narrowest length²)/2.

3.20. ALT and succinate levels measurement

Serum isolated from blood samples of mice on day 16 were used for ALT and succinate levels measurement. Bioassay systems' EnzyChromTM Alanine Transaminase Assay Kit (Cat# EALT-100) and EnzyChromTM Succinate Assay Kit (ESNT-100) were used according to manufacturer instructions.

3.21. Statistics

Statistical analysis calculations were carried out using Microsoft Excel and GraphPad Prism software 9.0. For each of the experiment, statistical analysis was performed separately. p-values <0.05 was considered statistically significant. All data is expressed in the form of mean \pm standard error unless otherwise specified. p-values are shown in the figure for each of the comparisons made, if * were used for depiction then following rules were applied – * = 0.033; **0.002; and *** < 0.001 (NEJM p-value style).

Author contributions

SI designed and performed experiments, analyzed data, and wrote the manuscript; NDN and AS assisted in cell culture and material characterization; APS and JLM performed animal experiments and cell culture; HSB and MDG performed polymer characterization *via* NMR spectroscopy and SEC and helped with manuscript editing; JRY performed confocal microscopy; STL, XS, TH and HG performed metabolomics experiments, TER and MC assisted with extracellular flux assays; APA designed experiments and wrote the manuscript.

Funding

The authors would also like to acknowledge the start-up funds provided by Arizona State University, and NIH 1R01AI155907-01, 1R01AR078343-01, 1R01GM144966-01, NSF award# 2145877 to APA for the completion of this study. HSB and MDG would like to thank the NSF (Award# 1836719) and ARPA-E (DE-AR0001103) for funding.

CRediT authorship contribution statement

Sahil Inamdar: Writing – original draft, Conceptualization. Abhirami P. Suresh: Investigation. Joslyn L. Mangal: Investigation. Nathan D. Ng: Investigation. Alison Sundem: Investigation. Hoda Shokrollahzadeh Behbahani: Investigation. Thomas E. Rubino: Investigation.

Xiaojian Shi: Investigation. Sharon T. Loa: Investigation. Jordan R. Yaron: Investigation. Taro Hitosugi: Supervision. Matthew Green: Supervision. Haiwei Gu: Supervision. Marion Curtis: Supervision. Abhinav P. Acharya: Supervision, Funding acquisition.

Declaration of Competing Interest

APA is affiliated with a start-up company, Immunometabolix, LLC. The PCT/US21/12691 "Central carbon metabolite-based polymers for Immunotherapy" have APA and SI as authors, which is under option by ImmunoMetabolix, LLC. There are no other conflicts to declare.

Data availability

The main data supporting the results of this study are available within the paper and its Supplementary Information. Source data for tumor growth curves are provided with this paper. The raw and analyzed datasets generated during the study are too large to be publicly shared, but they are available for research purposes from the corresponding author on reasonable request.

Acknowledgements

The authors would like to acknowledge the Flow Cytometry Core, the Regenerative Medicine Imaging Facility, the KED Genomics Core, Bioinformatics Core, the FEI at Erying Materials Center, the Advanced Light Microscopy Facilities, and the Department of Animal Care and Technologies at Arizona State University. Additionally, the authors would like to thank Dr. Seo, School of Molecular Sciences, Arizona State University for providing access to dynamic light scatter

Appendix A. Supplementary data

Supplementary data to this article can be found online at https://doi.org/10.1016/j.jconrel.2023.05.014.

References

- A. Luengo, D.Y. Gui, M.G. Vander Heiden, Targeting metabolism for Cancer therapy, cell, Chem. Biol. 24 (2017) 1161–1180, https://doi.org/10.1016/j. chembiol.2017.08.028.
- [2] M. Cerezo, S. Rocchi, Cancer cell metabolic reprogramming: a keystone for the response to immunotherapy, Cell Death Dis. 11 (2020) 964, https://doi.org/ 10.1038/s41419-020-03175-5.
- [3] N. Pacifici, A. Bolandparvaz, J.S. Lewis, Stimuli-responsive biomaterials for vaccines and immunotherapeutic applications, Adv. Ther. 3 (2020) 2000129, https://doi.org/10.1002/adtp.202000129.
- [4] J. Nam, S. Son, K.S. Park, W. Zou, L.D. Shea, J.J. Moon, Cancer nanomedicine for combination cancer immunotherapy, Nat. Rev. Mater. 4 (2019) 398–414, https:// doi.org/10.1038/s41578-019-0108-1.
- [5] B. Kelly, L.A. O'Neill, Metabolic reprogramming in macrophages and dendritic cells in innate immunity, Cell Res. 25 (2015) 771–784, https://doi.org/10.1038/ cr.2015.68.
- [6] E.J. Pearce, B. Everts, Dendritic cell metabolism, Nat. Rev. Immunol. 15 (2015) 18–29, https://doi.org/10.1038/nri3771.
- [7] J.L. Mangal, S. Inamdar, Y. Yang, X. Shi, M. Wankhede, H. Gu, K. Rege, M. D. Green, M. Curtis, A. Acharya, Metabolite releasing polymers control dendritic cell function by modulating their energy metabolism, J. Mater. Chem. B (2020), https://doi.org/10.1039/d0tb00790k.
- [8] A. Kulkarni, V. Chandrasekar, S.K. Natarajan, A. Ramesh, P. Pandey, J. Nirgud, H. Bhatnagar, D. Ashok, A.K. Ajay, S. Sengupta, A designer self-assembled supramolecule amplifies macrophage immune responses against aggressive cancer, Nat. Biomed. Eng. 2 (2018) 589–599, https://doi.org/10.1038/s41551-018-0254-6
- [9] J.L. Mangal, S. Inamdar, T. Le, X. Shi, M. Curtis, H. Gu, A.P. Acharya, Inhibition of glycolysis in the presence of antigen generates suppressive antigen-specific responses and restrains rheumatoid arthritis in mice, Biomaterials. 277 (2021), 121079, https://doi.org/10.1016/j.biomaterials.2021.121079.
- [10] N. Kedia-Mehta, D.K. Finlay, Competition for nutrients and its role in controlling immune responses, Nat. Commun. 10 (2019) 2123, https://doi.org/10.1038/ s41467-019-10015-4.
- [11] E.L. Pearce, E.J. Pearce, Metabolic pathways in immune cell activation and quiescence, Immunity. 38 (2013) 633–643, https://doi.org/10.1016/J. IMMUNI.2013.04.005.

- [12] K. Ganeshan, A. Chawla, Metabolic regulation of immune responses, Annu. Rev. Immunol. 32 (2014) 609–634, https://doi.org/10.1146/annurev-immunol-032713.120236
- [13] B. Everts, E. Amiel, S.C.C. Huang, A.M. Smith, C.H. Chang, W.Y. Lam, V. Redmann, T.C. Freitas, J. Blagih, G.J.W.V.D. Windt, M.N. Artyomov, R.G. Jones, E.L. Pearce, E.J. Pearce, TLR-driven early glycolytic reprogramming via the kinases TBK1-IKKe supports the anabolic demands of dendritic cell activation, Nat. Immunol. (2014), https://doi.org/10.1038/ni.2833.
- [14] M. Obaid, S. Udden, P. Alluri, S.S. Mandal, LncRNA HOTAIR regulates glucose transporter Glut1 expression and glucose uptake in macrophages during inflammation, Sci. Rep. 11 (2021) 1–19.
- [15] M. Jang, S.S. Kim, J. Lee, Cancer cell metabolism: implications for therapeutic targets, Exp. Mol. Med. 45 (2013), https://doi.org/10.1038/emm.2013.85 e45-e45.
- [16] M.G. Vander Heiden, L.C. Cantley, C.B. Thompson, Understanding the Warburg effect: the metabolic requirements of cell proliferation, Science. 324 (2009) 1029–1033, https://doi.org/10.1126/science.1160809.
- [17] M.V. Liberti, J.W. Locasale, The Warburg effect: how does it benefit Cancer cells? Trends Biochem. Sci. 41 (2016) 211–218, https://doi.org/10.1016/j. tibs.2015.12.001.
- [18] C.V. Dang, M. Hamaker, P. Sun, A. Le, P. Gao, Therapeutic Targeting of Cancer Cell Metabolism, 2011.
- [19] Y. Zhao, E.B. Butler, M. Tan, Targeting Cellular Metabolism to Improve Cancer Therapeutics, 2013.
- [20] H.C. Yoo, Y.C. Yu, Y. Sung, J.M. Han, Glutamine reliance in cell metabolism, Exp. Mol. Med. 52 (2020) 1496–1516, https://doi.org/10.1038/s12276-020-00504-8.
- [21] A.A. Cluntun, M.J. Lukey, R.A. Cerione, J.W. Locasale, Glutamine metabolism in cancer: understanding the heterogeneity, Trends Cancer 3 (2017) 169–180, https://doi.org/10.1016/j.trecan.2017.01.005.
- [22] M. Kodama, K. Oshikawa, H. Shimizu, S. Yoshioka, M. Takahashi, Y. Izumi, T. Bamba, C. Tateishi, T. Tomonaga, M. Matsumoto, K.I. Nakayama, A shift in glutamine nitrogen metabolism contributes to the malignant progression of cancer, Nat. Commun. 11 (2020) 1320, https://doi.org/10.1038/s41467-020-15136-9.
- [23] J.L. Messerschmidt, G.C. Prendergast, G.L. Messerschmidt, How cancers escape immune destruction and mechanisms of action for the new significantly active immune therapies: helping nonimmunologists decipher recent advances, Oncologist 21 (2016) 233–243, https://doi.org/10.1634/theoncologist.2015-0282.
- [24] N. Vasan, J. Baselga, D.M. Hyman, A view on drug resistance in cancer, Nature. 575 (2019) 299–309, https://doi.org/10.1038/s41586-019-1730-1.
- [25] C.A. Wicker, B.G. Hunt, S. Krishnan, K. Aziz, S. Parajuli, S. Palackdharry, W. R. Elaban, T.M. Wise-Draper, G.B. Mills, S.E. Waltz, V. Takiar, Glutaminase Inhibition with Telaglenastat (CB-839) Improves Treatment Response in Combination with Ionizing Radiation in Head and Neck Squamous Cell Carcinoma Models, 2021.
- [26] J.A.-O. Harding, M. Telli, P. Munster, M.A.-O. Voss, J.R. Infante, A. DeMichele, M. Dunphy, M.H. Le, C.A.-O. Molineaux, K. Orford, F. Parlati, S.H. Whiting, M. K. Bennett, N.M. Tannir, F. Meric-Bernstam, A phase 1 dose-escalation and expansion study of telaglenastat in patients with advanced or metastatic solid tumors, Clin. Cancer Res. (2021), https://doi.org/10.1158/1078-0432.CCR-21-1204. CCR-21-1204-E.2021 [pii] LID.
- [27] P.A.-O. Lee, D. Malik, N.A.-O. Perkons, P. Huangyang, S. Khare, S. Rhoades, Y.A.-O. Gong, M. Burrows, J.A.-O. Finan, I. Nissim, T.A.-O. Gade, A.M. Weljie, M. C. Simon, Targeting Glutamine Metabolism Slows Soft Tissue Sarcoma Growth, 2020.
- [28] P.S. Liu, H. Wang, X. Li, T. Chao, T. Teav, S. Christen, G.D. Conza, W.C. Cheng, C. H. Chou, M. Vavakova, C. Muret, K. Debackere, M. Mazzone, H.D. Huang, S. M. Fendt, J. Ivanisevic, P.C. Ho, α-Ketoglutarate orchestrates macrophage activation through metabolic and epigenetic reprogramming, Nat. Immunol. (2017), https://doi.org/10.1038/ni.3796.
- [29] N.M. Anderson, P. Mucka, J.G. Kern, H. Feng, The emerging role and targetability of the TCA cycle in cancer metabolism, protein, Cell. 9 (2018) 216–237, https://doi.org/10.1007/s13238-017-0451-1.
- [30] J. Connors, N. Dawe, J. Van Limbergen, The role of succinate in the regulation of intestinal inflammation, Nutrients. 11 (2018) 25, https://doi.org/10.3390/ nu11010025.
- [31] K.J. Harber, K.E. de Goede, S.G.S. Verberk, E. Meinster, H.E. de Vries, M. van Weeghel, M.P.J. de Winther, J. Van den Bossche, Succinate is an inflammationinduced immunoregulatory metabolite in macrophages, Metabolites. 10 (2020) 372. https://doi.org/10.3390/metabo10090372.
- [32] C. Nastasi, A. Willerlev-Olsen, K. Dalhoff, S.L. Ford, A.-S.Ø. Gadsbøll, T.B. Buus, M. Gluud, M. Danielsen, T. Litman, C.M. Bonefeld, C. Geisler, N. Ødum, A. Woetmann, Inhibition of succinate dehydrogenase activity impairs human T cell activation and function, Sci. Rep. 11 (2021) 1458, https://doi.org/10.1038/s41598-020-80933-7.
- [33] G.M. Tannahill, A.M. Curtis, J. Adamik, E.M. Palsson-Mcdermott, A.F. McGettrick, G. Goel, C. Frezza, N.J. Bernard, B. Kelly, N.H. Foley, L. Zheng, A. Gardet, Z. Tong, S.S. Jany, S.C. Corr, M. Haneklaus, B.E. Caffrey, K. Pierce, S. Walmsley, F. C. Beasley, E. Cummins, V. Nizet, M. Whyte, C.T. Taylor, H. Lin, S.L. Masters, E. Gottlieb, V.P. Kelly, C. Clish, P.E. Auron, R.J. Xavier, L.A.J. O'Neill, Succinate is an inflammatory signal that induces IL-1β through HIF-1α, Nature. (2013) https://doi.org/10.1038/nature11986.
- [34] G.L. Semenza, Regulation of Oxygen Homeostasis by Hypoxia-Inducible Factor 1, 2023.
- [35] E. Monferrer, S. Sanegre, I. Vieco-Martí, A. López-Carrasco, F. Fariñas, A. Villatoro, S. Abanades, S. Mañes, L. de la Cruz-Merino, R. Noguera, T. Álvaro Naranjo,

- Immunometabolism modulation in therapy, Biomedicines. 9 (2021) 798, https://doi.org/10.3390/biomedicines9070798.
- [36] C. Rosales, E. Uribe-Querol, Phagocytosis: a fundamental process in immunity, Biomed. Res. Int. 2017 (2017), https://doi.org/10.1155/2017/9042851, 9042851-9042851.
- [37] H. Wang, M.C. Sobral, D.K.Y. Zhang, A.N. Cartwright, A.W. Li, M.O. Dellacherie, C. M. Tringides, S.T. Koshy, K.W. Wucherpfennig, D.J. Mooney, Metabolic labeling and targeted modulation of dendritic cells, Nat. Mater. 19 (2020) 1244–1252, https://doi.org/10.1038/s41563-020-0680-1.
- [38] Q. Wei, Y. Qian, J. Yu, C.C. Wong, Metabolic rewiring in the promotion of cancer metastasis: mechanisms and therapeutic implications, Oncogene. 39 (2020) 6139–6156, https://doi.org/10.1038/s41388-020-01432-7.
- [39] J.V. Nayak, D.A. Hokey, A. Larregina, Y. He, R.D. Salter, S.C. Watkins, L.D. Falo, Phagocytosis induces lysosome remodeling and regulated presentation of particulate antigens by activated dendritic cells, J. Immunol. 177 (2006) 8493–8503
- [40] X. Shi, S. Wang, P. Jasbi, C. Turner, J. Hrovat, Y. Wei, J. Liu, H. Gu, Database-assisted globally optimized targeted mass spectrometry (dGOT-MS): broad and reliable metabolomics analysis with enhanced identification, Anal. Chem. 91 (2019) 13737–13745, https://doi.org/10.1021/acs.analchem.9b03107.
- [41] A.E. Rodriguez, G.S. Ducker, L.K. Billingham, C.A. Martinez, N. Mainolfi, V. Suri, A. Friedman, M.G. Manfredi, S.E. Weinberg, J.D. Rabinowitz, Serine metabolism supports macrophage IL-1β production, Cell Metab. 29 (2019), 1003-1011. e4.
- [42] A. Rehman, K.C. Hemmert, A. Ochi, M. Jamal, J.R. Henning, R. Barilla, J. P. Quesada, C.P. Zambirinis, K. Tang, M. Ego-Osuala, R.S. Rao, S. Greco, M. Deutsch, S. Narayan, H.L. Pachter, C.S. Graffeo, D. Acehan, G. Miller, Role of fatty-acid synthesis in dendritic cell generation and function, J. Immunol. (2013), https://doi.org/10.4049/jimmunol.1202312.
- [43] L.A.J. O'Neill, E.J. Pearce, Immunometabolism governs dendritic cell and macrophage function, J. Exp. Med. 213 (2015) 15–23, https://doi.org/10.1084/ jem.20151570.
- [44] I. Zanoni, R. Ostuni, G. Capuano, M. Collini, M. Caccia, A.E. Ronchi, M. Rocchetti, F. Mingozzi, M. Foti, G. Chirico, CD14 regulates the dendritic cell life cycle after LPS exposure through NFAT activation, Nature. 460 (2009) 264–268.
- [45] L. Biscari, C.D. Kaufman, C. Farré, V. Huhn, M.F. Pacini, C.B. Balbi, K.A. Gómez, A. R. Pérez, A. Alloatti, Immunization with lipopolysaccharide-activated dendritic cells generates a specific CD8+ T cell response that confers partial protection against infection with trypanosoma cruzi, Front. Cell. Infect. Microbiol. (2022) 066.
- [46] C. Bellio, C. DiGloria, D.R. Spriggs, R. Foster, W.B. Growdon, B.R. Rueda, The metabolic inhibitor CPI-613 negates treatment enrichment of ovarian cancer stem cells, Cancers. 11 (2019) 1678.
- [47] S.D. Stuart, A. Schauble, S. Gupta, A.D. Kennedy, B.R. Keppler, P.M. Bingham, Z. Zachar, A strategically designed small molecule attacks alpha-ketoglutarate dehydrogenase in tumor cells through a redox process, Cancer Metab. 2 (2014) 1–15
- [48] Z. Zachar, J. Marecek, C. Maturo, S. Gupta, S.D. Stuart, K. Howell, A. Schauble, J. Lem, A. Piramzadian, S. Karnik, Non-redox-active lipoate derivates disrupt cancer cell mitochondrial metabolism and are potent anticancer agents in vivo, J. Mol. Med. 89 (2011) 1137–1148.
- [49] X. Li, M. Wenes, P. Romero, S.C.-C. Huang, S.-M. Fendt, P.-C. Ho, Navigating metabolic pathways to enhance antitumour immunity and immunotherapy, Nat. Rev. Clin. Oncol. 16 (2019) 425–441, https://doi.org/10.1038/s41571-019-0203-7.
- [50] Z. Zaslona, L.A. O'Neill, Cytokine-like roles for metabolites in immunity, Mol. Cell 78 (2020) 814–823.
- [51] E. Mills, L.A.J. O'Neill, Succinate: a metabolic signal in inflammation, Trends Cell Biol. 24 (2014) 313–320, https://doi.org/10.1016/j.tcb.2013.11.008.
- [52] M.P. Murphy, L.A.J. O'Neill, Krebs cycle reimagined: the emerging roles of succinate and Itaconate as signal transducers, Cell. 174 (2018) 780–784, https:// doi.org/10.1016/j.cell.2018.07.030.
- [53] T. Wang, H. Liu, G. Lian, S.-Y. Zhang, X. Wang, C. Jiang, HIF1α-induced glycolysis metabolism is essential to the activation of inflammatory macrophages, Mediat. Inflamm. 2017 (2017), https://doi.org/10.1155/2017/9029327, 9029327–9029327
- [54] N. Kelley, D. Jeltema, Y. Duan, Y. He, The NLRP3 inflammasome: an overview of mechanisms of activation and regulation, Int. J. Mol. Sci. 20 (2019) 3328, https://doi.org/10.3390/ijms20133328.
- [55] D. Sharma, A. Malik, C. Guy, P. Vogel, T.-D. Kanneganti, TNF/TNFR axis promotes pyrin inflammasome activation and distinctly modulates pyrin inflammasomopathy, J. Clin. Invest. 129 (2019) 150–162, https://doi.org/ 10.1172/ICI121372
- [56] H. Daub, F.U. Weiss, C. Wallasch, A. Ullrich, Role of transactivation of the EGF receptor in signalling by G-protein-coupled receptors, Nature. 379 (1996) 557–560, https://doi.org/10.1038/379557a0.
- [57] W. Vermi, E. Giurisato, S. Lonardi, P. Balzarini, E. Rossi, D. Bosisio, S. Sozzani, W. Pellegrini, C. Doglioni, A. Marchetti, Ligand-dependent activation of EGFR in follicular dendritic cells sarcoma is sustained by local production of cognate ligands, Clin. Cancer Res. 19 (2013) 5027–5038.

- [58] P. Wee, Z. Wang, Epidermal growth factor receptor cell proliferation signaling pathways, Cancers. 9 (2017) 52.
- [59] B.A. Hemmings, D.F. Restuccia, Pi3k-pkb/akt pathway, Cold Spring Harb. Perspect. Biol. 4 (2012), a011189.
- [60] B. Kloeckener-Gruissem, K. Vandekerckhove, G. Nürnberg, J. Neidhardt, C. Zeitz, P. Nürnberg, I. Schipper, W. Berger, Mutation of solute carrier SLC16A12 associates with a syndrome combining juvenile cataract with microcornea and renal glucosuria, Am. J. Hum. Genet. 82 (2008) 772–779.
- [61] J.J. Castorino, S.M. Gallagher-Colombo, A.V. Levin, P.G. FitzGerald, J. Polishook, B. Kloeckener-Gruissem, E. Ostertag, N.J. Philp, Juvenile cataract-associated mutation of solute carrier SLC16A12 impairs trafficking of the protein to the plasma membrane, Invest. Ophthalmol. Vis. Sci. 52 (2011) 6774–6784.
- [62] P. Berraondo, M.F. Sanmamed, M.C. Ochoa, I. Etxeberria, M.A. Aznar, J.L. Pérez-Gracia, M.E. Rodríguez-Ruiz, M. Ponz-Sarvise, E. Castañón, I. Melero, Cytokines in clinical cancer immunotherapy, Br. J. Cancer 120 (2019) 6–15, https://doi.org/10.1038/s41416-018-0328-y.
- [63] D.S. Chen, I. Mellman, Elements of cancer immunity and the cancer-immune set point, Nature. 541 (2017) 321–330, https://doi.org/10.1038/nature21349.
- [64] D.S. Chen, I. Mellman, Oncology Meets Immunology: The Cancer-Immunity Cycle, 2013
- [65] Z.E. Stine, Z.T. Schug, J.M. Salvino, C.V. Dang, Targeting cancer metabolism in the era of precision oncology, Nat. Rev. Drug Discov. 1–22 (2021).
- [66] J.A. Champion, A. Walker, S. Mitragotri, Role of particle size in phagocytosis of polymeric microspheres, Pharm. Res. 25 (2008) 1815–1821, https://doi.org/ 10.1007/s11095-008-9562-y
- [67] Y.-A. Shen, C.-L. Chen, Y.-H. Huang, E.E. Evans, C.-C. Cheng, Y.-J. Chuang, C. Zhang, A. Le, Inhibition of glutaminolysis in combination with other therapies to improve cancer treatment, Curr. Opin. Chem. Biol. 62 (2021) 64–81.
- [68] M.B. Bloom, D. Perry-Lalley, P.F. Robbins, Y. Li, M. El-Gamil, S.A. Rosenberg, J. C. Yang, Identification of tyrosinase-related protein 2 as a tumor rejection antigen for the B16 melanoma, J. Exp. Med. 185 (1997) 453–459, https://doi.org/10.1084/jem.185.3.453.
- [69] M. Mansour, B. Pohajdak, W.M. Kast, A. Fuentes-Ortega, E. Korets-Smith, G. M. Weir, R.G. Brown, P. Daftarian, Therapy of established B16-F10 melanoma tumors by a single vaccination of CTL/T helper peptides in VacciMax®, J. Transl. Med. 5 (2007) 20. https://doi.org/10.1186/1479-5876-5-20.
- [70] A.M. Manicone, J.K. McGuire, Matrix metalloproteinases as modulators of inflammation, Semin. Cell Dev. Biol. 19 (2007) 34–41.
- [71] S.T. Reddy, A. Rehor, H.G. Schmoekel, J.A. Hubbell, M.A. Swartz, In vivo targeting of dendritic cells in lymph nodes with poly(propylene sulfide) nanoparticles, J. Control. Release (2006), https://doi.org/10.1016/j.jconrel.2006.01.006.
- [72] A. Schudel, D.M. Francis, S.N. Thomas, Material design for lymph node drug delivery, Nat. Rev. Mater. 4 (2019) 415–428, https://doi.org/10.1038/s41578-019-0110-7
- [73] J.J.P. van Beek, G. Flórez-Grau, M.A.J. Gorris, T.S.M. Mathan, G. Schreibelt, K. F. Bol, J. Textor, I.J.M. de Vries, Human pDCs Are Superior to cDC2s in Attracting Cytolytic Lymphocytes in Melanoma Patients Receiving DC Vaccination, 2020.
- [74] H. Kasler, E. Verdin, How inflammaging diminishes adaptive immunity, Nat. Aging 1 (2021) 24–25, https://doi.org/10.1038/s43587-020-00021-3.
- [75] M.D.D. Buck, D. O'Sullivan, R.I.I.K. Geltink, J.D.D. Curtis, C.H. Chang, D.E. E. Sanin, J. Qiu, O. Kretz, D. Braas, G.J.J.W. van der Windt, Q. Chen, S.C.C. Huang, C.M.M. O'Neill, B.T.T. Edelson, E.J.J. Pearce, H. Sesaki, T.B.B. Huber, A.S. S. Rambold, E.I.L. Pearce, Mitochondrial dynamics controls T cell fate through metabolic programming, Cell. (2016), https://doi.org/10.1016/j.cell.2016.05.035.
- [76] C.-H. Chang, J. Qiu, D. O'Sullivan, M.D. Buck, T. Noguchi, J.D. Curtis, Q. Chen, M. Gindin, M.M. Gubin, G.J.W. van der Windt, E. Tonc, R.D. Schreiber, E.J. Pearce, E.L. Pearce, Metabolic competition in the tumor microenvironment is a driver of Cancer progression, Cell. 162 (2015) 1229–1241, https://doi.org/10.1016/J. CELL.2015.08.016.
- [77] R.I.K. Geltink, D. O'Sullivan, M. Corrado, A. Bremser, M.D. Buck, J.M. Buescher, E. Firat, X. Zhu, G. Niedermann, G. Caputa, B. Kelly, U. Warthorst, A. Rensing-Ehl, R.L. Kyle, L. Vandersarren, J.D. Curtis, A.E. Patterson, S. Lawless, K. Grzes, J. Qiu, D.E. Sanin, O. Kretz, T.B. Huber, S. Janssens, B.N. Lambrecht, A.S. Rambold, E. J. Pearce, E.L. Pearce, Mitochondrial priming by CD28, Cell. 171 (2017), https://doi.org/10.1016/j.cell.2017.08.018, 385–397.e11.
- [78] E.L. Pearce, M.C. Walsh, P.J. Cejas, G.M. Harms, H. Shen, L.S. Wang, R.G. Jones, Y. Choi, Enhancing CD8 T-cell memory by modulating fatty acid metabolism, Nature. 460 (2009) 103–107, https://doi.org/10.1038/nature08097.
- [79] A.P. Acharya, N.V. Dolgova, C.Q. Xia, M.J. Clare-Salzler, B.G. Keselowsky, Adhesive substrates modulate the activation and stimulatory capacity of non-obese diabetic mouse-derived dendritic cells, Acta Biomater. (2011), https://doi.org/ 10.1016/j.actbio.2010.08.026.
- [80] A.P. Acharya, M.J. Clare-Salzler, B.G. Keselowsky, A high-throughput microparticle microarray platform for dendritic cell-targeting vaccines, Biomaterials. 30 (2009) 4168–4177, https://doi.org/10.1016/j. biomaterials.2009.04.032.
- [81] A.P. Acharya, M.R. Carstens, J.S. Lewis, N. Dolgova, C.Q. Xia, M.J. Clare-Salzler, B. G. Keselowsky, A cell-based microarray to investigate combinatorial effects of microparticle-encapsulated adjuvants on dendritic cell activation, J. Mater. Chem. B (2016), https://doi.org/10.1039/c5tb01754h.